Received 10 September 2024
Revised 29 September 2024
Accepted 29 September 2024

Eddy current quantitative evaluation of high-speed railway contact wire cracks based on neural network

Xueying Zhou, Wentao Sun, Zehui Zhang and Junbo Zhang
Railway Science and Technology Research and Development Center, China Academy of Railway Sciences Corporation Limited, Beijing, China
Haibo Chen
Power Supply Department, China Railway Zhengzhou Group Corporation Limited, Zhengzhou, China, and
Hongmei Li
Railway Science and Technology Research and Development Center, China Academy of Railway Sciences Corporation Limited, Beijing, China

Abstract

Purpose – The purpose of this study is to study the quantitative evaluation method of contact wire cracks by analyzing the changing law of eddy current signal characteristics under different cracks of contact wire of high-speed railway so as to provide a new way of thinking and method for the detection of contact wire injuries of high-speed railway.

Design/methodology/approach – Based on the principle of eddy current detection and the specification parameters of high-speed railway contact wires in China, a finite element model for eddy current testing of contact wires was established to explore the variation patterns of crack signal characteristics in numerical simulation. A crack detection system based on eddy current detection was built, and eddy current detection voltage data was obtained for cracks of different depths and widths. By analyzing the variation law of eddy current signals, characteristic parameters were obtained and a quantitative evaluation model for crack width and depth was established based on the back propagation (BP) neural network.

Findings – Numerical simulation and experimental detection of eddy current signal change rule is basically consistent, based on the law of the selected characteristics of the parameters in the BP neural network crack quantitative evaluation model also has a certain degree of effectiveness and reliability. BP neural network training results show that the classification accuracy for different widths and depths of the classification is 100 and 85.71%, respectively, and can be effectively realized on the high-speed railway contact line cracks of the quantitative evaluation classification.

Originality/value – This study establishes a new type of high-speed railway contact wire crack detection and identification method, which provides a new technical means for high-speed railway contact wire injury detection. The study of eddy current characteristic law and quantitative evaluation model for different cracks in contact line has important academic value and practical significance, and it has certain guiding significance for the detection technology of contact line in high-speed railway.

Keywords High-speed railway catenary, Crack detection, Eddy current detection, Neural network

Paper type Research paper

"Science and Technology Research and Development Program Project of China Railway Group Co., Ltd", classification code J2022G016.

Railway Sciences
Vol. 3 No. 6, 2024
pp. 764-778
Emerald Publishing Limited
e-ISSN: 2755-0915
p-ISSN: 2755-0907
DOI 10.1108/RS-09-2024-0038

1. Introduction

Contact wire is an important wire in the contact network of high-speed railroads which is directly involved in the current receiving of the bow network and is an important part of electrified railroads, and its quality and operational status directly affect the quality of the current receiving of the bow network and the safe transportation of electrified railroads (Wu & Li, 2021). In recent years, with the operation of many high-speed railroads entering or exceeding the 10-year period, the contact network equipment gradually enters the fatigue operation period, especially the contact wires, after years of dynamic action of the bow network and electrical erosion, its performance and status gradually decline. With the increasing mileage of China's high-speed railroad operation, the requirements for high-speed railroad operation safety are also increasing and the fatigue life of contact wire in the contact network is an important index that affects the safety of high-speed train operation. Once the contact line fatigue fracture occurs, it will directly affect the normal power supply of high-speed trains and pose a serious threat to the operation safety of trains (Li, Wei, & Dai, 2024).

Early detection of contact line damage can effectively reduce the rate of contact network accidents, especially the rate of major accidents. However, the contact line is high-altitude and high-voltage equipment, it is difficult to find defects in the wire by manual inspection, and modern detection technology must be used, and at present there is no contact line damage detection equipment, and it can only be avoided through the frequent change of the line at regular intervals to avoid the breakage of the contact line, which will cause a great deal of manpower, material resources and waste of days and windows.

Existing equipment damage detection techniques usually include penetration testing, magnetic particle testing, radiographic testing, ultrasonic testing, image testing and eddy current testing. Compared with other inspection techniques, eddy current inspection technology has the advantages of being fast, convenient, non-polluting, low cost, non-contact measurement, high sensitivity to defects on and near the surface of the body being inspected, especially suitable for inspecting small-sized objects and convenient for on-site inspection, etc. It is more suitable for contact wires which have the characteristics of copper, are close to the cylindrical shape and have a small cross-sectional area (generally 120 mm^2, 150 mm^2, etc.) wire (Sun, 2005).

At present, domestic and foreign researchers and scholars for eddy current detection technology have related research. Yang Binfeng *et al.* of the National University of Defense Technology (NUDT) conducted inspection and testing of machined simulated aircraft multilayer structure specimens by means of a pulsed eddy current inspection system. The German BAM and Eurailscout companies use eddy current technology as a compensation technology for ultrasonic testing in the detection of rail tread damage (Thomas, Heckel, & Hanspach, 2007; Pohl, Erhard, Montag, Thomas, & Wüstenberg, 2004). Prof. Guiyun Tian *et al.* of Newcastle University, UK, studied eddy current pulse thermography in multi-crack imaging reconstruction of rail tread (Wilson, Tian, Mukriz, & Almond, 2011). Domestic scholars Xiong and other scholars have used the back propagation (BP) neural network model to identify the depth and angle of rail cracks, and the final crack depth and angle classification accuracy is higher than the curve fitting model classification accuracy (Xiong, Zhang, & Ma, 2021). Choi and Ashour *et al.* utilized the support vector machine algorithm to identify the defective regions to accomplish the defect recognition task. However, image preprocessing can take a lot of time, and the algorithm is difficult to model and migrate defect features completely due to the diversity of defects and has poor reusability (Choi, Jeon, Lee, Yun, & Kim, 2014; Ashour, Khalid, Halin, Abdullah, & Darwish, 2018).

In metal pipelines, LIU S.J. *et al.* extracted the magnetic memory detection signals of cracks in metal pipelines and constructed a BP neural network to effectively quantitatively identify the crack parameters of pipelines (Liu, Li, Jiang, & He, 2017). WANGZ.W. *et al.* obtained the relationship between crack depth, width and detection signal through numerical

simulation and experimental study and realized high-precision inversion of cracks using BP neural network based on genetic algorithm (Wang, Fei, Ye, Qiu, & Woo, 2020). Recognition study of pipeline defects using an IPSO-RBF neural network improves the recognition accuracy of morphological features of oil and gas pipeline defects (Zhang & Yu, 2017).

However, the existing eddy current inspection research mainly focuses on the inspection of oil pipelines, aircraft fuselage structure, steel or the inspection of a special-purpose material, without applying eddy current inspection to contact wire injury detection. For the contact wire injury, it is still time-consuming and inefficient to inspect the wire defects by manual inspection. In this paper, we explore the characteristic law of the eddy current detection signal of a contact line crack through finite element simulation, use the eddy current detection system to collect the detection signal of artificial injury on the surface of the rail and use a neural network model to identify the size of cracks, which provides a new technical means for the detection of contact wire injury in high-speed railway.

2. Numerical simulation

2.1 Theoretical analysis of eddy current detection

Eddy current flaw detection is based on the principle of electromagnetic induction, the use of alternating magnetic field close to the conductor material or the conductor material in the magnetic field when the conductor material movement produces vortex-like currents (eddy currents), at the same time vortex-like currents flow in the conductor material and the formation of an inverse magnetic field, the inverse magnetic field and the original magnetic field to form a dynamic equilibrium, when there are uneven and discontinuous materials in the workpiece, the inverse magnetic field changes to break the dynamic equilibrium, making the detection coil voltage and impedance changes, so as to achieve the purpose of defect detection. Dynamic equilibrium, so that the detection coil voltage and impedance change, so as to achieve the purpose of defect detection.

The specific principle is shown in Figure 1. When the excitation coil passes into the alternating excitation signal, according to Ampere's law, the coil will produce an alternating primary magnetic field H_1, assuming that the magnetic induction strength of the magnetic field at a point in space is B_1, and its direction can be judged by the right-hand spiral rule. According to Faraday's law of electromagnetic induction, when the alternating primary magnetic field is applied to the test specimen, an induced eddy current I_1 will be generated inside the test specimen, and the eddy current will generate an eddy current magnetic field H_2, whose magnetic induction strength is B_2. Since the pipes are mostly ferromagnetic

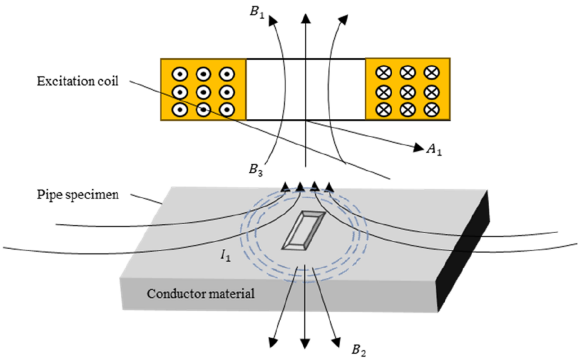

Figure 1.
Eddy current detection schematic

Source(s): Authors' own work

materials, when the primary magnetic field H_1 generated by the coil is applied on the test specimen's surface, the internal magnetic domains of the specimen rotate in the direction of the field H_1 and a field with the same direction as the primary magnetic field is also generated produce a magnetized magnetic field H_3 with the same direction as the primary magnetic field, and its magnetic induction strength is B_3. A magnetic chip is placed at the detection point A_1, and at this time, the composite magnetic induction strength B detected by the magnetic chip in space is the vector sum of B_1, B_2 and B_3. The value of B can be determined by Equation (1).

$$B = B_1 + B_2 + B_3 \tag{1}$$

where B_1 is the alternating primary magnetic induction intensity; B_2 is the eddy current magnetic induction intensity and B_3 is the magnetization magnetic induction intensity.

When there is a crack in the test piece, the primary magnetic field of coil excitation remains unchanged; the crack prevents the eddy current from forming a loop, thus making the eddy current larger and the eddy current magnetic field increases; at the same time, the crack will weaken the specimen magnetization, resulting in a decrease in the magnetized magnetic field due to the direction of the eddy current magnetic field and magnetized magnetic field is opposite to the direction of the magnetic field and the magnetized magnetic field is much larger than the eddy current magnetic field, so the magnetized magnetic field will offset the eddy current magnetic field. Finally, the magnetic signal change of this compound field will lead to the change of detection coil voltage and impedance. In this paper, the change of detection voltage is used to determine the crack size of the tested part.

2.2 Finite element model

At present, the main use is copper contact wire, as shown in Figure 2. A finite element simulation model of the contact wire is established to study the influence of crack size on the eddy current detection signal. The model uses a contact wire with a cross-sectional area of 150 mm^2, as shown in Figure 3, and the specific specification parameters are shown in Table 1.

Based on the specification parameters of the contact line in the above table, a three-dimensional model for eddy current detection of cracks in the contact line is established, as shown in Figure 4, which mainly includes the excitation coil, cracks, specimen and air domain, and the material of the specimen is copper-magnesium alloy (magnesium content of 0.5%). The

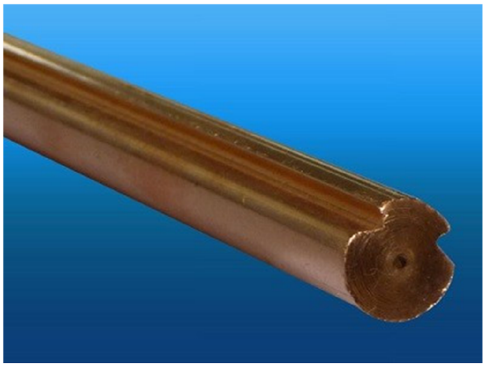

Source(s): Authors' own work

Figure 2.
Copper alloy contact wire physical picture

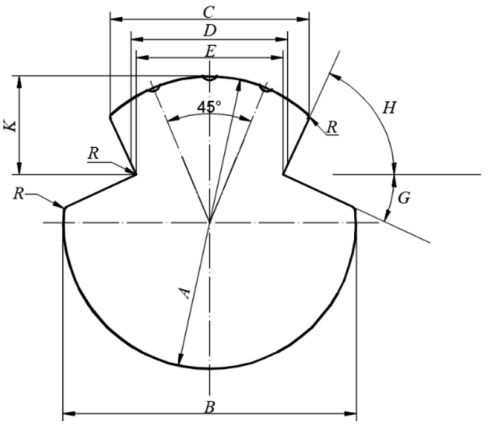

Figure 3.
Schematic cross-section of copper alloy contact wire

Source(s): Chinese Mechanical Engineering Society of Non-Destructive Testing (1986)

Nominal cross-sectional area (mm^2)			150
Dimensions and tolerances (mm)	A	±1%	14.4
	B	±2%	14.4
	C	±2%	9.71
	D	−2%+4%	7.24
	E		6.8
	K		4
	R		0.4
Angle and deviation (°)	G	±1	27
	H		51
Unit mass (kg/km)			1,350

Table 1.
Copper alloy contact wire specification table

Source(s): Chinese Mechanical Engineering Society of Non-Destructive Testing (1986)

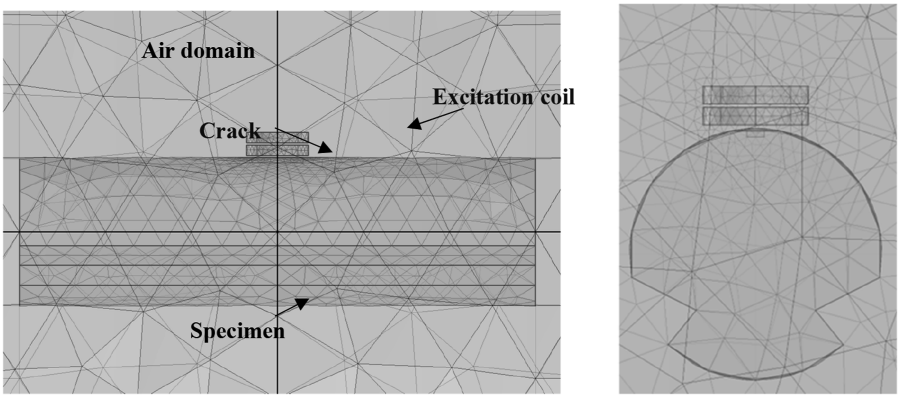

front view
(a)

side view
(b)

Figure 4.
Three-dimensional model for eddy current detection of cracks in contact wires

Source(s): Authors' own work

size of the excitation coil is set to six mm outer diameter, four mm inner diameter, one mm thickness, 20 turns and 0.5 mm lift-off. The frequency of the excitation current signal is 30 kHz.

2.3 Simulation results

Seven cracks with different widths are set up, with a length of 10 mm, a depth of 0.2 mm, a width of 0.1–0.7 mm (step size 0.1) mm and a spacing of 20 mm between adjacent cracks. The excitation coil is scanned along the horizontal direction of the contact line, and the voltage signal of the detection coil is extracted to intercept the simulated signals of each crack on the scanning path, and the results are shown in Figure 5.

As can be seen from Figure 5, the simulation signal of the excitation coil in the crack-free region is basically unchanged, which is approximately a horizontal straight line, and the distribution of the signal is consistent with the surface morphology of the specimen; the simulation signal through the cracked region undergoes an obvious sudden change, which is presented as an "M" shape; when the coil starts to approach the cracked region, the detected voltage signal increases gradually and then starts to decrease gradually when approaching the center of the crack. When the coil starts to approach the cracked area, the detected voltage signal gradually increases and then gradually decreases when approaching the cracked center and reaches the lowest at the cracked center; after the coil passes the cracked center, the signal starts to increase, and then the signal gradually decreases until it returns to the approximate horizontal straight line when the coil is out of the cracked area; the values of peaks and valleys of the wave increase with the increase of the width, and the spacing of the peaks and peaks of the signal does not have any obvious change.

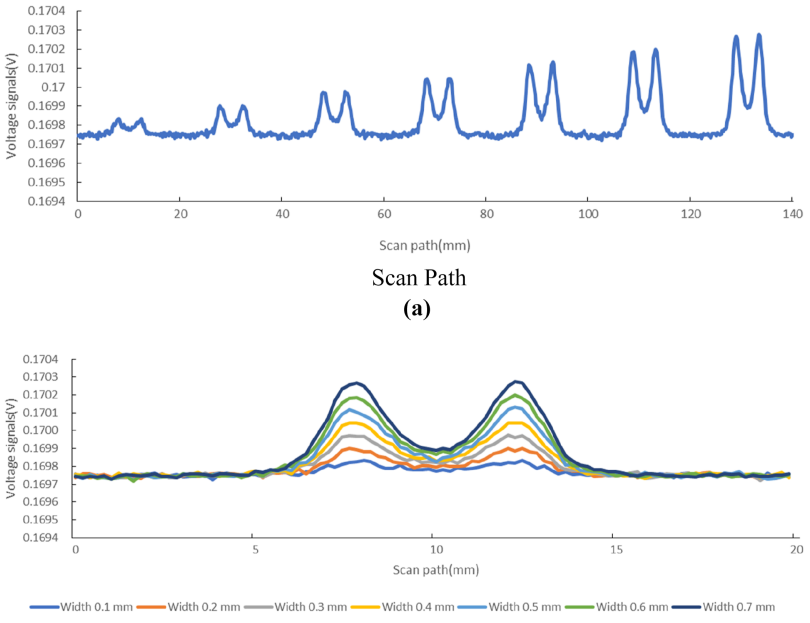

Source(s): Authors' own work

Figure 5.
Simulation signals for cracks of different widths

Seven cracks with different depths are set up, with a length of 10 mm, a width of 0.2 mm, a depth of 0.1~0.7 mm (step 0.1) mm and a spacing of 20 mm between adjacent cracks. The excitation coil is scanned along the horizontal direction of the contact line, and the voltage signals of the detection coil are extracted, and the simulated signals of each crack on the scanning path are intercepted, and the results are shown in Figure 6.

As can be seen from Figure 6, the simulation signal of the excitation coil in the crack-free region is basically unchanged, approximately a horizontal straight line, and the signal distribution is consistent with the surface topography of the specimen; the coil starts to approach the crack region and the detection voltage signal gradually increases. When the width is 0.1~0.6 mm, the signal begins to decrease gradually when approaching the crack center and reaches the lowest at the crack center; the signal begins to increase after the coil passes through the crack center. When the width is 0.7 mm, the value of the signal wave valley at the crack center disappears, and at this time is the wave peak value. When the coil is driving out of the cracked area, the signal gradually decreases again until it returns to an approximate horizontal straight line; the peak and trough values increase with the increase in width, and there is no significant change in the spacing between the signal peaks and peaks.

3. Experimental verification

3.1 Specimen preparation

As with the model in the numerical simulation, the copper-magnesium alloy contact wire was selected as a specimen, as shown in Figure 7. Cracks with a length of 10 mm, a depth of

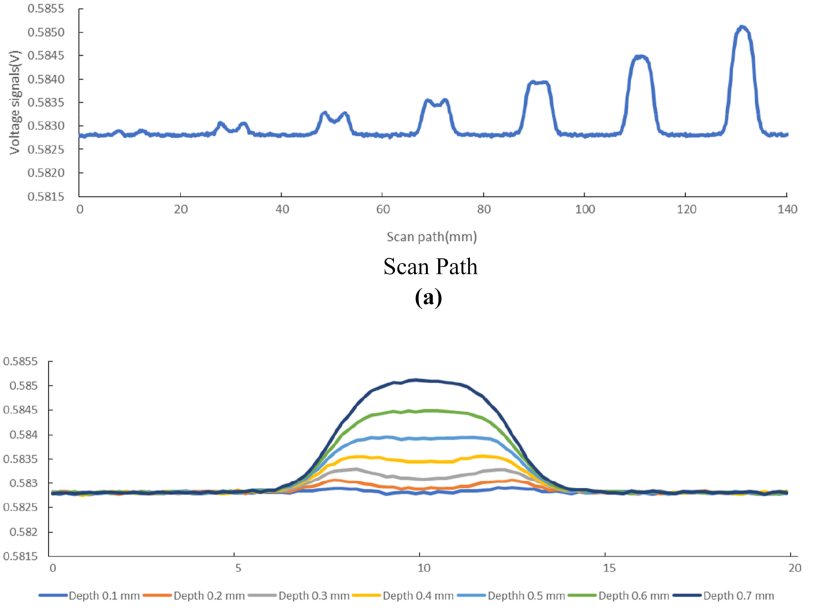

Figure 6.
Simulation signals for cracks of different depths

Source(s): Authors' own work

Profile of crack specimens of different widths

(a)

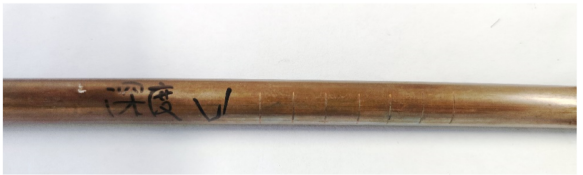

Profile of crack specimens of different depths

(b)

Source(s): Authors' own work

Figure 7.
Specimen shape

0.2 mm, a width of 0.1–0.7 mm (step size 0.1 mm) and a depth of 0.1–0.7 mm (step size 0.1 mm) were processed in the specimen at certain intervals.

3.2 Test platforms

A crack eddy current detection test system is constructed to test and verify the cracks of different sizes, and the parameters of the test probe are consistent with the simulation. The test system device is shown in Figure 8, the specimen is placed on the test bench, the probe is fixed on the horizontal moving slide, the horizontal moving slide drives the probe to realize the scanning movement in the path above the specimen, the eddy current sensor located at the bottom of the probe converts the extracted magnetic field signal into a voltage signal and outputs it through the transmission cable to the acquisition card inside the industrial computer, and then transforms it into a digital signal to be transmitted to the acquisition

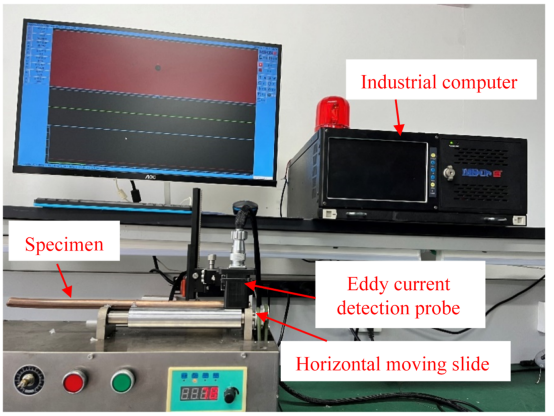

Source(s): Authors' own work

Figure 8.
Test system unit

program after amplification and filtering process. After amplification and filtering, the signal is transformed into a digital signal and transferred to the acquisition program, which is finally analyzed, processed and displayed in the acquisition program.

3.3 Test results and analysis

The probe was scanned along the path at 0.5 mm above the different cracked specimens, the peak of the detection voltage signal was extracted and the detection signal of each crack was intercepted, and the results are shown in Figure 9.

Analyzing Figure 9(a), it can be seen that due to different degrees of vibration during the operation of the test bench and the influence of the surface roughness of the specimen, the detection signal is not like the symmetrical "M shape" in the numerical simulation, but the overall undulation trend and the simulation signal are consistent. The peak value rises with the increase of crack width and is lowest in the region of 0.1 mm depth (1.10 V) and reaches the peak in the region of 0.7 mm depth (19.57 V); the trough value also rises with the increase of crack width and is lowest in the region of 0.1 mm depth (0.16 V) and reaches the peak in the region of 0.7 mm depth (5.56 V).

Analyzing Figure 9(b), it can be seen that the overall undulation trend of the detected signal is basically consistent with the simulated signal. The peak value rises with the increase of crack depth, and is lowest in the region of 0.1 mm depth (1.29 V), and reaches the peak in the region of 0.7 mm depth (9.18 V); the trough value also rises with the increase of crack depth, and is lowest in the region of 0.1 mm depth (0.12 V), and reaches the peak in the region of 0.7 mm depth (5.19 V). Again, due to the different degrees of vibration during the operation of the test bench and the influence of the surface roughness of the specimen, coupled with the fact that the deeper the depth of the laser engraving, the greater the error,

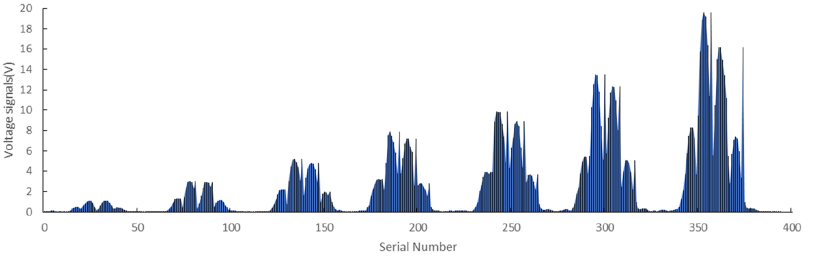

Different widths

(a)

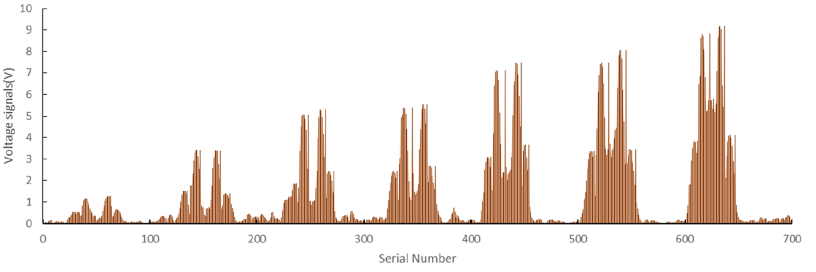

Different depths

(b)

Source(s): Authors' own work

Figure 9.
Crack detection signals

the rate of increase of the trough value in the test is not as high as that in the simulation signal, and there is still a trough value at a depth of 0.7 mm.

4. Quantitative crack identification based on BP neural network

4.1 Feature parameter extraction

The quantitative identification of the crack signal is closely related to the selection of its characteristic parameters, through the comparative analysis of simulation and experimental eddy current detection signals, combined with the characteristics of the BP neural network, this paper adopts the peak value (V_{max}), peak-to-peak value (V_z), circumference (C) and area (S) as the characteristic parameters of the crack signal of the contact line, shown in Figure 10.

(1) The peak value of the signal in the crack region of the sample V_{max}. $V_{max} = V_m - V_j$, where V_j is the baseline value of the test signal.

(2) Sample crack center region signal peak value V_z. $V_z = V_m - V_n$, where V_n is the test signal crack center region valley value.

(3) Test sample crack region signal perimeter C. $C = \sum_{i=a}^{b} \sqrt{(x_{i+1} - x_i)^2 + (V_{i+1} - V_i)^2}$, where x is the value of the scanning path of the test signal, V_i is the value of the voltage of the test signal and a and b are the start and end positions of the scanning path of the test signal, respectively.

(4) Signal area of the cracked region of the specimen S. $S = \sum_{i=a}^{b} \frac{(V_{i+1} + V_i - 2V_j)(x_{i+1} - x_i)}{2}$.

4.2 BP neural network

Classification of crack width and depth were classified, respectively, and the BP neural network model was used to classify and train the injury parameters, and the width and depth were classified into seven classes, and the crack classification training level table is shown in Table 2.

The training model uses a BP neural network. A BP neural network consists of three parts: an input layer, a hidden layer and an output layer and its network structure is shown in Figure 11.

The learning process of a BP neural network consists of forward propagation of information and backward propagation of error, the core of which is to continuously adjust the network parameters, i.e. weights and thresholds, by passing the error backward while correcting it in order to realize or approximate the desired input–output mapping relationship.

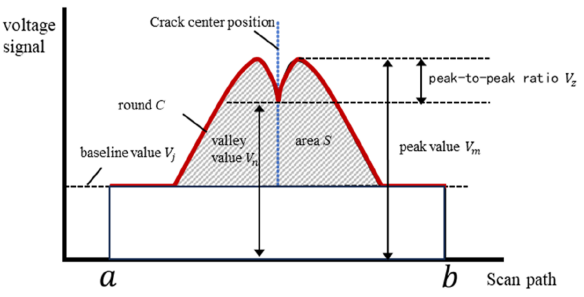

Source(s): Authors' own work

Figure 10.
Crack detection signals of different widths

4.2.1 Crack width evaluation. Each crack with different widths was detected 21 times, respectively, and a total of 147 groups of crack signal feature values were extracted from seven cracks and 20 groups were randomly selected as training samples and one group as a training sample from the 21 groups of samples for each crack, which were divided into 140 groups of training samples and seven groups of test samples. Among them, seven groups of test samples are shown in Table 3.

The extracted crack eigenvalues of different widths are used as inputs to the BP neural network. The cracks corresponding to each group of feature values are categorized according to Table 2, and the output corresponding to the categorization is used as the output of the BP neural network. The BP neural network designed above was trained using 140 sets of training data to obtain the width evaluation model. The cross-entropy loss curve during training is shown in Figure 12.

Table 2. Crack classification training scale

Crack width classification		Crack depth classification	
Width/mm	Classification corresponding output	Depth/mm	Classification corresponding output
0.1	1	0.1	1
0.2	2	0.2	2
0.3	3	0.3	3
0.4	4	0.4	4
0.5	5	0.5	5
0.6	6	0.6	6
0.7	7	0.7	7

Source(s): Authors' own work

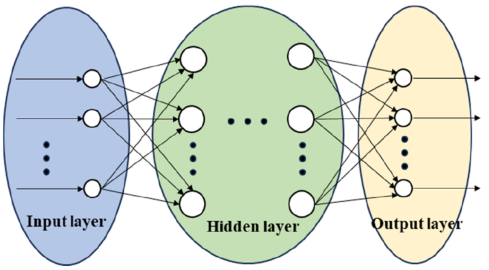

Figure 11. BP neural network diagram

Source(s): Authors' own work

Table 3. Characterization parameters of test samples at different widths

Serial no.	Width/mm	Peak value/V	Peak-to-peak value/V	Round/mm	Area/mm^2
1	0.1	0.98	0.76	97.39915	30.78505
2	0.2	2.79	2.09	102.2378	95.38318
3	0.3	5.15	4.19	109.1269	166.6636
4	0.4	7.45	5.03	117.8188	252.028
5	0.5	10	6.78	129.4612	330.1869
6	0.6	13.35	7.79	140.1176	451.1215
7	0.7	19.17	11.46	180.4781	628.2336

Source(s): Authors' own work

4.2.2 Crack depth evaluation. About 11 inspections were conducted for each crack with different depths, respectively, and a total of 77 sets of crack signal feature values were extracted for the seven cracks, which were divided into 70 sets of training data and seven sets of test data. Among them, seven groups of test samples are shown in Table 4.

About 11 inspections were carried out for each crack of different depths, respectively, and a total of 77 sets of crack signal feature values were extracted for the seven cracks, and 10 sets of 11 samples were randomly selected as training samples and 1 set of 11 samples were randomly selected as training samples for each crack, which were divided into 70 sets of training data and seven sets of test data. Among them, seven groups of test samples are shown in Table 4.

The extracted crack feature values of different depths are used as inputs to the BP neural network. The cracks corresponding to each group of feature values are categorized according to Table 2, and the output corresponding to the categorization is used as the output of the BP neural network. The BP neural network designed above was trained using 70 sets of training data to obtain the depth evaluation model. The cross-entropy loss curve during training is shown in Figure 13.

4.3 Crack identification results and analysis

BP neural network training was used to obtain the crack width evaluation model, seven groups of test samples were verified, and the results of the categories to which the crack width belonged are shown in Table 5, and the accuracy of the trained neural network model for the quantitative evaluation of the width of the seven groups of test data was 100% for the classification.

BP neural network training was used to obtain the crack depth evaluation model, seven groups of test samples were verified, and the results of the categories to which the crack depth belongs were obtained as shown in Table 6, and the classification accuracy of the

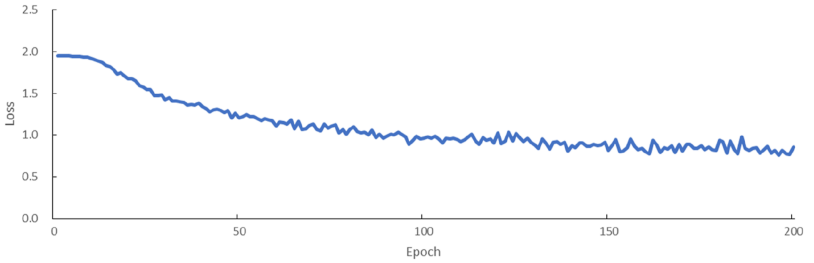

Source(s): Authors' own work

Figure 12.
Training loss curves with different widths

Serial no.	Width/mm	Peak value/V	Peak-to-peak value/V	Round/mm	Area/mm2
1	0.1	1.29	1.17	183.5322	66.03738
2	0.2	3.42	3.05	190.3993	179.215
3	0.3	5.3	4.88	198.1522	258.271
4	0.4	5.54	5.19	199.7663	274.3458
5	0.5	7.46	6.83	211.0284	336.2336
6	0.6	8.08	7.4	214.058	384.8037
7	0.7	9.18	8.45	218.8534	413.5421

Source(s): Authors' own work

Table 4.
Characterization parameters of test samples at different depths

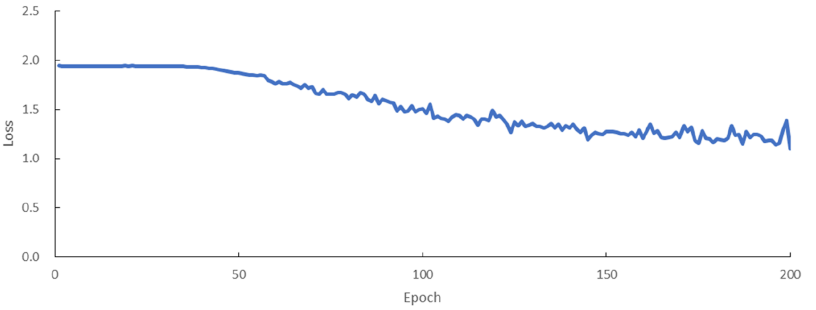

Figure 13.
Training loss curves with different depths

Source(s): Authors' own work

Serial no.	Width/mm	Actual category	Neural network results
1	0.1	1	1
2	0.2	2	2
3	0.3	3	3
4	0.4	4	4
5	0.5	5	5
6	0.6	6	6
7	0.7	7	7
Breadth quantitative evaluation of classification accuracy/%			100

Table 5.
Comparison of classification results for quantitative evaluation of neural network widths

Source(s): Authors' own work

Serial no.	Width/mm	Actual category	Neural network results
1	0.1	1	1
2	0.2	2	2
3	0.3	3	3
4	0.4	4	3
5	0.5	5	5
6	0.6	6	6
7	0.7	7	7
Breadth quantitative evaluation of classification accuracy/%			85.71

Table 6.
Comparison of classification results for quantitative evaluation of neural network depths

Source(s): Authors' own work

trained neural network model for the quantitative evaluation of the depth of seven groups of test samples was 85.71%.

5. Conclusion

(1) This paper establishes a finite element model for eddy current detection of contact line and derives the variation rules of crack signal characteristics of different sizes under numerical simulation. In the absence of cracks in the region when the simulation signal is basically no significant changes, approximately a horizontal straight line

passes through the cracked region when the simulation signal changes significantly, showing the "M-shaped."

(2) This paper builds the contact line crack eddy current detection test system, through the system detected signal change rule and simulation signal is basically the same, and according to the rule of change, selected four characteristic parameters as the input of BP neural network model.

(3) This paper establishes the BP neural network crack quantitative evaluation model for different width and depth of the classification accuracy of 100 and 85.71% and can effectively realize the high-speed railway contact line crack quantitative evaluation classification.

The research results of this paper provide a new technical means for contact line damage detection of high-speed railways, which can make the damage detection of contact wire avoid the inefficiency caused by the way of purely relying on manual inspection and improve the efficiency of contact wire damage detection. Future research can further consider a more automated, intelligent way to carry out the detection of contact wire and improve the diversity of the detection content, not only to realize the identification of cracks but also to include the contact wire wear, internal defects and so on.

References

Ashour, M. W., Khalid, F., Halin, A. A., Abdullah, L. L., & Darwish, S. H. (2018). Surface defects classification of hot-rolled steel strips using multi-directional shearlet features. *Arabian Journal for Science and Engineering*, *44*(4), 2925–2932. doi: 10.1007/S13369-018-3329-5.

Chinese Mechanical Engineering Society of Non-Destructive Testing (1986). *Eddy current inspection*. Mechanical Industry Press.

Choi, D. C., Jeon, Y. J., Lee, S. J., Yun, J. P., & Kim, S. W. (2014). Algorithm for detecting seam cracks in steel plates using a gabor filter combination method. *Applied Optics*, *53*(22), 4865–4872. doi: 10.1364/ao.53.004865.

Li, X., Wei, Y., & Dai, L. (2024). Research on the fatigue life of high-speed railway contact WireBased on measured pantograph-catenary contact force. *China Railway Science*, *45*(4), 168–179.

Liu, S. J., Li, S. L., Jiang, M., & He, D. (2017). Quantitative identification of pipeline crack based on bp neural network. *Key Engineering Materials*, *737*, 477–480. doi: 10.4028/www.scientific.net/kem.737.477.

Pohl, R., Erhard, A., Montag, H. J., Thomas, H. M., & Wüstenberg, H. (2004). Ndt techniques for railroad wheel and gauge corner inspection. *NDT and E International*, *37*(2), 89–94. doi: 10.1016/j.ndteint.2003.06.001.

Sun, X. (2005). *Eddy Current Testing Application in railway catenary's defect*. Chengdu: Southwest Jiaotong University.

Thomas, H. M., Heckel, T., & Hanspach, G. (2007). Advantage of a combined ultrasonic and eddy current examination for railway inspection trains. *Insight: Non-Destructive Testing and Condition Monitoring*, *49*(6), 341–344. doi: 10.1784/insi.2007.49.6.341.

Wang, Z., Fei, Y., Ye, P., Qiu, F., & Woo, W. L. (2020). Crack characterization in ferromagnetic steels by pulsed eddy current technique based on ga-bp neural network model. *Journal of Magnetism and Magnetic Materials*, *500*, 166412. doi: 10.1016/j.jmmm.2020.166412.

Wilson, J., Tian, G., Mukriz, I., & Almond, D. (2011). Pec thermography for imaging multiple cracks from rolling contact fatigue. *NDT and E International*, *44*(6), 505–512. doi: 10.1016/j.ndteint.2011.05.004.

Wu, W., & Li, X. (2021). Study on electrical factors of dropper breakage in high-speed railway catenary. *China Railway Science*, *42*(2), 164–172.

Xiong, L., Zhang, Y., & Ma, Y. (2021). Characteristics evaluation of RCF crack on rail surface based on eddy current testing and neural network. *China Railway Science*, *42*(05), 69–75.

Zhang, H., & Yu, X. (2017). Research on oil and gas pipeline defect recognition based on ipso for rbf neural network. *Sustainable Computing: Informatics and Systems*, *20*, 203–209. doi: 10.1016/j.suscom.2017.08.002.

Corresponding author
Xueying Zhou can be contacted at: zhouxueaying@126.com